Steel and Composite Structures, *Vol. 26, No. 2 (2018) 227-239*
DOI: https://doi.org/10.12989/scs.2018.26.2.227

A design approach of integral-abutment steel girder bridges for maintenance

WooSeok Kim [1a], Yoseok Jeong [1b] and Jaeha Lee [*2]

[1] *Department of Civil Engineering, Chungnam National University, 99 Daehak-ro, Yuseong-gu, Daejeon 34134, Korea*
[2] *Department of Civil Engineering, Korea Maritime and Ocean University, 727 Taejong-ro, Yeongdo-Gu, Busan 49112, Korea*

(*Received March 21, 2017, Revised September 29, 2017, Accepted January 05, 2018*)

Abstract. Integral abutment bridges (IABs) have no joint across the length of bridge and are therefore also known as jointless bridges. IABs have many advantages, such as structural integrity, efficiency, and stability. More importantly, IABs have proven to be have both low maintenance and construction costs. However, due to the restraints at both ends of the girder due to the absence of a gap (joint), special design considerations are required. For example, while replacing the deck slabs to extend the service life of the IAB, the buckling strength of the steel girder without a deck slab could be much smaller than the case with deck slab in place. With no deck slab, the addition of thermal expansion in the steel girders generates passive earth pressure from the abutment and if the applied axial force is greater than the buckling strength of the steel girders, buckling failure can occur. In this study, numerical simulations were performed to estimate the buckling strength of typical steel girders in IABs. The effects of girder length, the width of flange and thickness of flange, imperfection due to fabrication and construction errors on the buckling strengths of multiple and single girders in IABs are studied. The effect of girder spacing, span length ratio (for a three span girder) and self-weight effects on the buckling strength are also studied. For estimation of the reaction force of the abutment generated by the passive earth pressure of the soil, BA 42/96 (2003), PennDOT DM4 (2015) and the LTI proposed equations (2009) were used and the results obtained are compared with the buckling strength of the steel girders. Using the selected design equations and the results obtained from the numerical analysis, equations for preventing the buckling failure of steel girders during deck replacement for maintenance are presented.

Keywords: bridge; buckling; construction; maintenance

1. Introduction

Integral abutment bridges (IABs) have no joint across the length of the bridge, and are therefore also known as jointless bridges. IABs have been built and successfully operated for several decades, especially in the U.S. and Europe, because of their many benefits. IABs have many advantages, such as structural integrity, efficiency, and stability. More importantly, IABs have proven to have low maintenance and construction costs. However, due to the restraints at both ends of the girder special design considerations are in need. For example, while replacing the deck slabs to extend the service life of IABs, the buckling strength of the steel girders without the deck slab could be much smaller than the strength with the deck slab present. With the addition of thermal expansion in the steel girders with no deck slab, a passive earth pressure from the abutment will be generated and if the generated axial force is greater than the buckling strength of the steel girders, buckling failures could occur. Many experimental and numerical studies have shown that IABs are influenced by thermal expansion, bridge length and soil stiffness (Laman and Kim 2009, Frosch *et al*. 2009, Ahn *et al*. 2011, Kim and Laman 2012, Civjan *et al*. 2013, Faraji *et al*. 2001, Dicleli and Albhasi 2004a, b, Pugasap *et al*. 2009, Baptiste *et al*. 2011).

By recent studies from LaFave *et al*. (2016) and William *et al*. (2012), it was also found that the bridge expansion is 90% of free expansion and determined mostly by thermal coefficients of materials used in girders.

In particular, the superstructure experiences a cyclic axial force and bending moment due to thermal movement over a bridge service life. The results from this research have led to a set of design equations (Kim *et al*. 2012, Kim and Laman 2013, Lee *et al*. 2016). NCHRP 20-07/106 report (2002) states that improperly predicting the thermal movement of an integral bridge may cause abutment damage and this movement may lead to severe damage if it is not properly designed for integral construction.

One component of the superstructure in an IAB, the deck slab, carries significant axial forces due to the thermal expansion of the superstructure in service conditions. However, unlike conventional jointed bridges, during deck replacement for maintenance, girders remain fixed at both abutments and the abutment is in contact with the backfill. In this fixed condition, the steel girders of IABs are subjected to significant axial forces during thermal expansion and could finally buckle along their weak axis as shown in Fig. 1.

Fig. 1 shows deformed shape of a girder due to thermal expansion during deck replacement. In this study, numerical simulations were performed to estimate the buckling

∗Corresponding author, Ph.D., Associate Professor,
E-mail: jaeha@kmou.ac.kr
[a] Ph.D., Associate Professor
[b] Ph.D., Post-doctoral Researcher

http://www.techno-press.org/?journal=scs&subpage=6 ISSN: 1229-9367 (Print), 1598-6233 (Online)

Fig. 1 Buckled steel girder of an IAB, MI, USA

strength of the typical steel girders in IABs. The effects of girder length, flange width and thickness, imperfections due to fabrication and construction errors on the buckling strengths of multiple and single girders in IABs were studied. In analytical program, the imperfection is used to superposition of buckling eigenmodes obtained from buckling analysis. The scale factor (%) used in this study is relative structural dimension. In this study, it is defined as deformation values of each mode shape multiplied by an associated scale factor. The girder spacing, span length ratio (for three span girders) and self-weight effects on the buckling strength of the steel girder were also studied. A parametric study for varying these key parameters was performed and regression curve fits into the analysis results were found. Finally, equations predicting the buckling of girders were proposed. For estimation of the reaction force of the abutment generated by the passive earth pressure of the backfill, design guidelines such as BA 42/96 (2003), PennDOT DM4 (2015) and the LTI (2009) equations were used and compared with the buckling strength of the steel girders. Field research by Lemnitzer *et al.* (2012) to estimate the passive earth pressure coefficient (K_p) were also referenced. Backfill pressure distribution along the height of the abutment from BA 42/96 (2003) could be found from Lock (2002).

2. Description of the numerical model

To develop the numerical model, a commercial finite element program, Abaqus 6.13 (Standard) was used. For the material properties, typical steel properties were used, with an elastic modulus of 205 GPa, Poisson’s ratio of 0.3 and a yield stress of 520 MPa. Steel hardening behavior was also considered in the model for the post-buckling analysis. For the buckling analysis, only the elastic material properties were considered, while the post-buckling analysis uses the elastic-plastic hardening behavior of the steel.

2.1 Dimensions of steel girders and boundary conditions

The steel girders of an IAB for this study are shown in Fig. 2. The typical type of steel girder for 120 m bridge was selected. The steel girders of the IAB were modeled using Abaqus 6.13, however no deck was considered, since it was removed for deck replacement.

The steel girder is a 122 m (40.5 m + 40.8 m + 40.5 m) long, three span continuous beam. Fig. 2 shows the cross

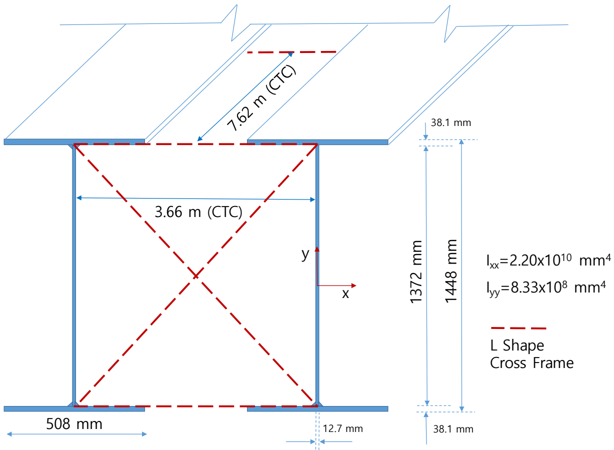

Fig. 2 Typical cross sectional shape of the steel girders

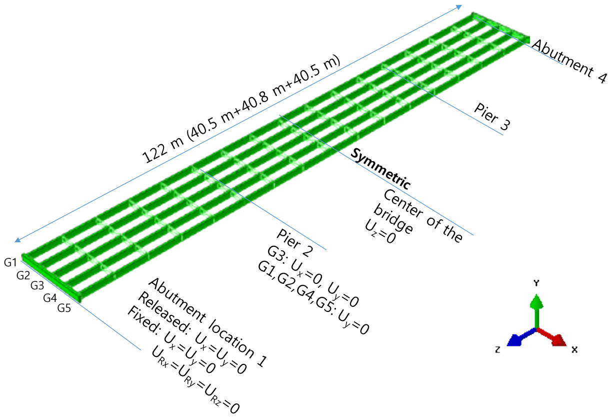

Fig. 3 Superstructure model of the IAB

section of the selected IAB. The girder spacing is 3.66 m and the total number of girders is five. The boundary conditions at the ends of the steel girders were considered as either fixed or released. If the backwall constraint is removed during deck replacement, the boundary conditions at both ends could be considered as being free to rotate. However, in general, a semi-fixed condition would be a practical boundary condition for IABs. In this study, both fixed and released boundary conditions are considered. Fig. 3 summarizes the boundary conditions for each location. The supports of girder 3 (G3) at the pier locations were transversely (x-axis) and vertically (y-axis) restrained, but were released in the longitudinal direction of the bridge. Other support locations of the remaining girders (G1, G2, G4, G5) were vertically (y-axis) restrained, with other boundary conditions as released.

Four node shell elements (S4R) were utilized in the model with reduced integration and a relatively fine mesh (approximately 0.125 m). The cross-frame between the girders was also included in the model by adding truss elements tied to the girders, with no buckling analysis considered for the cross-frames.

2.2 Analysis of the steel girders in IABs

In order to estimate the buckling strength and displacement depending on the axial force generated at both

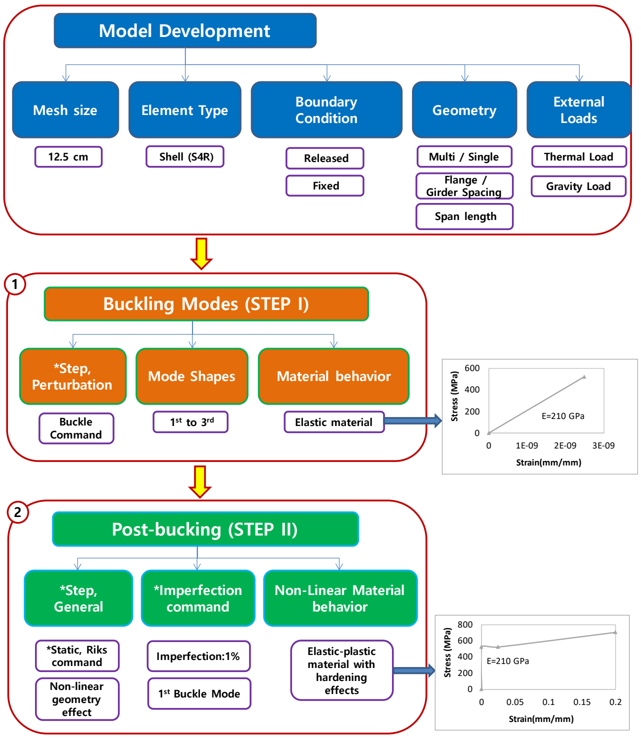

Fig. 4 The buckling analysis procedure conducted in study

abutments, a two step analysis was considered as shown in Fig. 4. Firstly, the model was developed as previously outlined and the number of girders, flange geometry, girder spacing and span length were selected as the key parameters. For the loading conditions, thermal loading and gravity load were considered. The other main loads in the bridge such as truck wheel load (live load) were not considered due to the deck replacement condition.

The first analysis stage (Step I) is a buckling analysis. Many buckling mode shapes could be obtained from this step. If the girder has a long length and small moment of inertia about the weak axis ($I_{weak\text{-}axis}$), sinusoidal buckling shapes are normally obtained. However, girders with a relatively short length and large moment of inertia would exhibit local buckling rather than a global sinusoidal shape. In this study, buckling mode shapes up to the 3rd were calculated based on the assumption that the main buckling modes are obtained mostly from the lower order. In this step, the linear material behavior (elastic material properties) were only considered based on the assumption that a small amount of deformation for the initial buckled shape would not cause any plastic strain in the steel girders. However, in the post-buckling analysis with displacement control (Step II), elasto-plastic behavior with hardening effects for the steel material was considered.

After completion of the buckling analysis, a post-buckling analysis was performed using predefined data from the buckled shape obtained from Step I.

In order to perform a post-buckling analysis, the Riks method (Riks 1972, 1979, Wempner 1971) was utilized. The Riks method is a load-deflection analysis and is useful when both the load and displacement are unknown and the failure type is an unstable collapse, such as a buckling failure.

For the Riks algorithm in Abaqus, the initial arc length increment needs to be designated. The initially suggested arc length increment is 0.01. Other input parameters for the Riks method, such as the total arc-length and the minimum and maximum arc length increments along the static equilibrium path are 1.0, 1E-05 and 1.0, respectively. It was confirmed that the load proportional factors are within a reasonable scope and the solution was well converged, when the selected parameters for utilizing the Riks method were used.

In the post buckling analysis using the Riks method, non-linear material properties were considered and a level of imperfection based on the previous buckling analysis was defined as an initial condition.

3. Analysis results from Step I (Elastic buckling mode analysis)

Firstly, a single girder analysis was performed and then a multi-girder IAB analysis was conducted in order to study the coupling effect between girders under the buckling loads and the interaction of the three continuous spans. Firstly, a single girder with a short length (40 m) and another with a long length (200 m) were studied to examine the behaviors from the length of the girder.

3.1 Buckling modes of single girder

The single girder analysis was performed with two boundary conditions (released for rotation, and fixed for rotation). Since the buckling behavior is primarily static behavior, only a limited number of dominant buckling modes, up to the 3rd mode, were investigated.

Fig. 5 shows the buckling shapes of the long single girder (40 m) with one span. Fulcrum positions for single girder are located at both ends. The first two mode shapes obtained from both the released and fixed boundary conditions exhibit similar shapes, except for the areas close to the ends. However, the 3rd mode shapes differ depending on the boundary conditions. While the released condition exhibits sinusoidal buckling shapes, the fixed condition shows lateral torsional buckling.

3.2 Buckling modes of the multi-girder system

After conducting the single girder analysis, a three-span continuous multi-girder system was analyzed with two boundary conditions (released or fixed about rotation) in order to compare the mode shapes with those from the single girder.

Fig. 6 shows the results from the buckling mode analysis of the long multi-girder system. The abutments at both ends and the supports are shown as lines in Fig. 6. For long multi-girders, as expected global sinusoidal buckling shapes were obtained rather than local buckling. As in the previous single girder cases, the mode shapes of the long multi-girders exhibited similar buckling shapes. It is noteworthy that regardless of the boundary conditions at both ends, the buckling shape of the center span exhibited

(a) 1st mode, released


(b) 1st mode, fixed


(c) 2nd mode, released


(d) 2nd mode, fixed


(e) 3rd mode, released

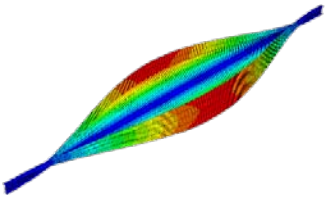
(f) 3rd mode, fixed

Fig. 5 Buckling mode analysis of a long single girder (40 m)

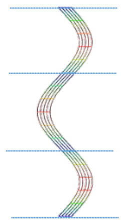
(a) 1st mode, released

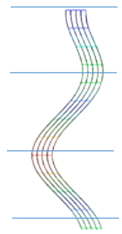
(b) 1st mode, fixed

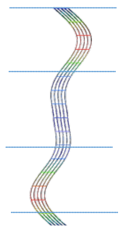
(c) 2nd mode, released

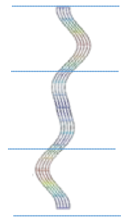
(d) 2nd mode, fixed

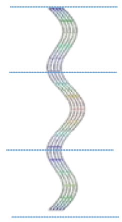
(e) 3rd mode, released

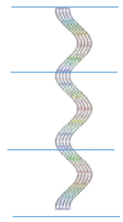
(f) 3rd mode, fixed

Fig. 6 Buckling mode analysis of a long multi-girder system (40.5 + 40.8 + 40.5 = 122 m)

a similar shape to that of the single girder. However, the 2nd and 3rd mode shapes of the center span in the multi-girder system are different from those of the single girder.

Interestingly, the buckling shape of the center span for the 2nd mode exhibits a relatively more straight line, while the other two spans exhibit global sinusoidal buckling shapes. For the 3rd buckling shape of the center span, while the single girders exhibited one and half cycle sinusoidal shapes, the center span of the multi-girder system exhibited one cycle of a sinusoidal shape. From this comparison, it can be concluded that depending on the boundary effects from the adjacent span, the number of cycles in the critical span could be varied.

Furthermore, unlike in a single girder 3rd buckling mode with a fixed boundary condition, there was no torsional buckling due to coupling effects between the girders. This indicates that if the mode 1 buckling shape only is

Table 1 Maximum buckling strength of a single girder

	Single girder											
BC*	BL (m)	SL (m)	IL (%)	FW (m)	FT (mm)	GS (m)	SLR (m/m)	SW	λ_c	A_{one} (m^2)	I_{yy} (m^4)	Normalized strength
R**	39	13	1	0.5	38	-	1	-	1.80	0.0554	0.0008	0.1837
	60	20	1	0.5	38	-	1	-	2.71	0.0554	0.0008	0.0961
	81	27	1	0.5	38	-	1	-	3.61	0.0554	0.0008	0.0546
	120	40	1	0.5	38	-	1	-	5.41	0.0554	0.0008	0.0239
	159	53	1	0.5	38	-	1	-	7.22	0.0554	0.0008	0.0135
	180	60	1	0.5	38	-	1	-	8.12	0.0554	0.0008	0.0104
F***	39	13	1	0.5	38	-	1	-	1.23	0.0554	0.0008	0.7996
	60	20	1	0.5	38	-	1	-	1.89	0.0554	0.0008	0.4798
	81	27	1	0.5	38	-	1	-	2.56	0.0554	0.0008	0.2724
	120	40	1	0.5	38	-	1	-	3.79	0.0554	0.0008	0.1257
	159	53	1	0.5	38	-	1	-	2.05	0.0554	0.0008	0.0699
	180	60	1	0.5	38	-	1	-	5.68	0.0554	0.0008	0.0548

*Indicate boundary condition; ** Indicate released at both ends; *** Indicate fixed at both ends

Table 2 Maximum buckling strength of multi-girders

Multi_girder system												
BC*	BL (m)	SL (m)	IL (%)	FW (m)	FT (mm)	GS (m)	SLR (m/m)	SW	λ_c	A_{one} (m^2)	I_{yy} (m^4)	Normalized strength
R**	40	13	1	0.5	38	3.67	1	-	1.80	0.0554	0.0008	0.3045
	80	27	1	0.5	38	3.67	1	-	3.61	0.0554	0.0008	0.0743
	120	40	1	0.5	38	3.67	1	-	5.41	0.0554	0.0008	0.0336
	160	53	1	0.5	38	3.67	1	-	7.22	0.0554	0.0008	0.0181
	200	67	1	0.5	38	3.67	1	-	9.02	0.0554	0.0008	0.0088
	120	40	1	0.25	38	3.67	1	-	12.49	0.0364	0.0001	0.0067
	120	40	1	0.5	38	3.67	1	-	5.41	0.0554	0.0008	0.0336
	120	40	1	0.75	38	3.67	1	-	3.44	0.0744	0.00266	0.0830
	120	40	1	1	38	3.67	1	-	2.50	0.0934	0.00632	0.1566
	120	40	1	0.5	19	3.67	1	-	6.25	0.0364	0.00039	0.0252
	120	40	1	0.5	38	3.67	1	-	5.41	0.0554	0.0008	0.0336
	120	40	1	0.5	57	3.67	1	-	5.16	0.0744	0.00118	0.0378
	120	40	1	0.5	76	3.67	1	-	5.00	0.0934	0.00158	0.0404
	120	40	0	0.5	38	3.67	1	-	5.41	0.0554	0.0008	0.0336
	120	40	0.01	0.5	38	3.67	1	-	5.41	0.0554	0.0008	0.0336
	120	40	0.1	0.5	38	3.67	1	-	5.41	0.0554	0.0008	0.0336
	120	40	1	0.5	38	3.67	1	o	5.41	0.0554	0.0008	0.0361
	120	40	1	0.5	38	1.83	1	-	5.41	0.0554	0.0008	0.0336
	120	40	1	0.5	38	5.49	1	-	5.41	0.0554	0.0008	0.0336
	120	40	1	0.5	38	3.67	0.5	-	5.41	0.0554	0.0008	0.0809
	120	40	1	0.5	38	3.67	2.0	-	5.41	0.0554	0.0008	0.0806
F***	40	13	1	0.5	38	3.67	1	-	1.26	0.0554	0.0008	0.7991
	80	27	1	0.5	38	3.67	1	-	2.53	0.0554	0.0008	0.1102
	120	40	1	0.5	38	3.67	1	-	3.79	0.0554	0.0008	0.0502
	160	53	1	0.5	38	3.67	1	-	5.05	0.0554	0.0008	0.0286
	200	67	1	0.5	38	3.67	1	-	6.32	0.0554	0.0008	0.0129
	120	40	1	0.25	38	3.67	1	-	8.74	0.0364	9.8E-05	0.0098
	120	40	1	0.5	38	3.67	1	-	3.79	0.0554	0.0008	0.0502
	120	40	1	0.75	38	3.67	1	-	2.41	0.0744	0.00266	0.1248
	120	40	1	1	38	3.67	1	-	1.75	0.0934	0.00632	0.2151
	120	40	1	0.5	19	3.67	1	-	4.37	0.0364	0.00039	0.0373
	120	40	1	0.5	38	3.67	1	-	3.79	0.0554	0.0008	0.0502
	120	40	1	0.5	57	3.67	1	-	3.61	0.0744	0.00118	0.0565
	120	40	1	0.5	76	3.67	1	-	3.50	0.0934	0.00158	0.0603
	120	40	0	0.5	38	3.67	1	-	3.79	0.0554	0.0008	0.6138
	120	40	0.01	0.5	38	3.67	1	-	3.79	0.0554	0.0008	0.2451
	120	40	0.1	0.5	38	3.67	1	-	3.79	0.0554	0.0008	0.1497
	120	40	1	0.5	38	3.67	1	o	5.41	0.0554	0.0008	0.0502
	120	40	1	0.5	38	1.83	1	-	5.41	0.0554	0.0008	0.0501
	120	40	1	0.5	38	5.49	1	-	5.41	0.0554	0.0008	0.0502
	120	40	1	0.5	38	3.67	0.5	-	5.41	0.0554	0.0008	0.1249
	120	40	1	0.5	38	3.67	2.0	-	5.41	0.0554	0.0008	0.1249

*Indicate boundary condition; ** Indicate released at both ends; *** Indicate fixed at both ends considered, the AISC single column buckling equation could be used for estimating the buckling strength of IAB steel girder bridges (multi-girders).

In this study, since it was found that the 1st mode buckling shape of the center span of multi-girders are similar to those of a single girder regardless of the boundary conditions, 1st mode buckling shapes only were considered for the post buckling analysis. If a buckling load due to thermal expansion occurs suddenly, the 2nd and 3rd mode should be considered, however, thermal expansion could be considered quasi-static behavior and this is a more realistic assumption. Therefore, the 1st mode could be enough for this study.

4. Post-buckling analysis

In this section, the results obtained from the post-buckling analysis with predefined data from the 1st buckling analysis are shown. Both a single girder and a multi-girder analysis have been conducted. A parametric study of the span length, imperfection level, flange width, flange thickness, girder spacing, span length ratio and self-weight was conducted and compared with the obtained results.

4.1 Maximum capacity of a single girder

Table 1 shows the obtained maximum buckling load, stress and normalized strength depending on various span length. BL and SL indicate bridge length and span length respectively. Likewise, GS, SLR and SW indicate girder spacing, span length ratio and self-weight respectively. For a single girder, the imperfection level (IL), flange width (FW), and flange thickness (FT) are fixed values as shown in Table 1. Normalized strength was calculated by dividing the maximum stress by yield stress of the steel.

As expected, the largest buckling strength (max. stress in Table 1) was obtained from the shortest length and fixed condition (13 m span length with fixed boundary conditions). In this case, the buckling strength is 415.78 MPa, while the yield strength of the girder is around 520 MPa.

4.2 Maximum capacity of multiple girder system

Table 2 shows the obtained maximum buckling load, stress and normalized strength depending on various key parameters.

4.2.1 Cross-frame effects

The multi-girder system includes cross-frame effects which are the interaction between the girders could be one of key factors in controlling buckling failure.

Cross-frame stresses were therefore investigated. The stress of the cross-frame, which is dependent on the moment of inertia about the weak axis of the girder section, was between 27.6 MPa and 74.7 MPa for a bridge length of 200 m. For released condition, cross-frames located at both ends exhibited the largest stress (74.7 MPa), while for the fixed condition cross-frames located at the pier locations exhibited the largest stress (27.6 MPa). It is thought that for the 200 m bridge, the sinusoidal global buckling shape affects the locations of the maximum stress. More importantly, most cross-frame exhibited a very low stress level (less than 6.2 MPa and 2.3 MPa respectively), indicating that cross-frame effects could be negligible because most steel plate girders are designed to support the vertical loads and thus the moment of inertia about the weak axis of the girder section is relatively small compared to the moment of inertia about the strong axis.

4.2.2 Comparison of multi-girder system with single girder

The buckling strength of the multi-girder is shown in Table. 2. The key parameter for controlling the buckling strength is the span length. Therefore, an analysis of results for the buckling strength per girder of a single and multi-girder system, as shown in Table 2, is shown in Fig. 7 against the span length. For the released condition (Fig. 7(a)), the multi-girder exhibited a larger maximum load for a short length, however, the difference decreases as the span length is increased. However, the fixed condition exhibits the opposite behavior, as the difference between the single and multi-girder was the smallest when the span length is the shortest. The buckling strength for the multi-girder showed a relatively smaller maximum axial load.

These differences between the two boundary conditions can be explained as for fixed case the single girder has an effective length factor (K) of 0.5, while the multi-girder is 0.7 with the two edge spans and 1.0 for the center span as shown in Fig. 8. Therefore, the buckling strength for the multi-girder system in a released condition exhibited a larger strength, while the axial strength for a multi-girder in the fixed condition exhibited a lower value compared to the single girder. For a quick and conservative estimation of the

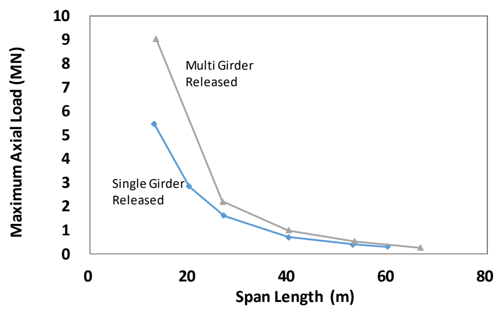

(a) Released condition

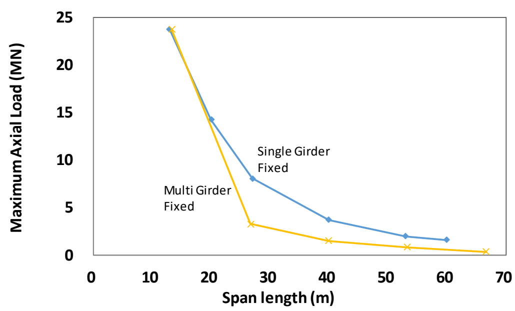

(b) Fixed condition

Fig. 7 Comparison of maximum axial load for a single and multi-girder against the girder length

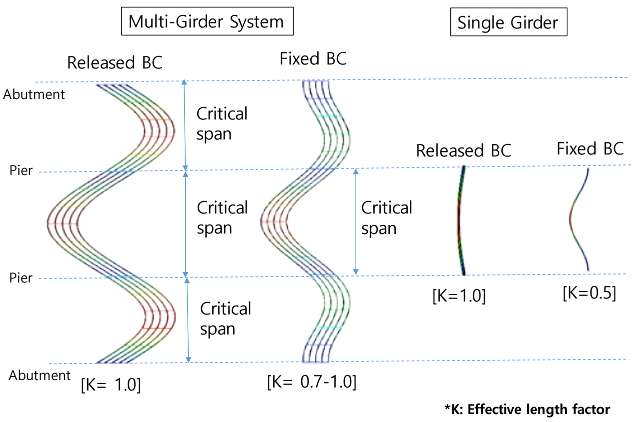

Fig. 8 Effective length factors under different conditions

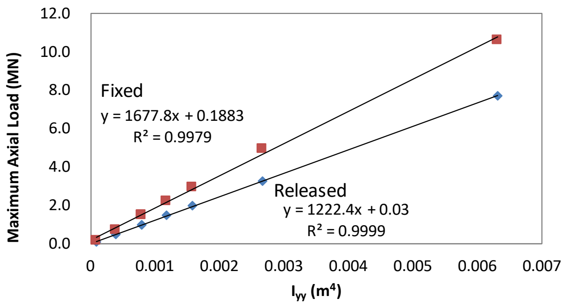

(a) Maximum axial load vs I_{yy}

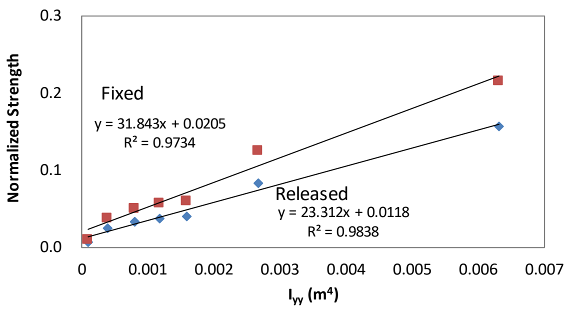

(b) Normalized strength vs I_{yy}

Fig. 9 Effect of I_{yy} on the buckling strength

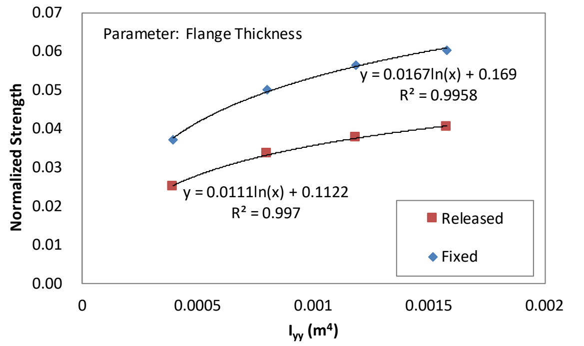

(a) Normalized strength vs I_{yy} varied by flange thickness

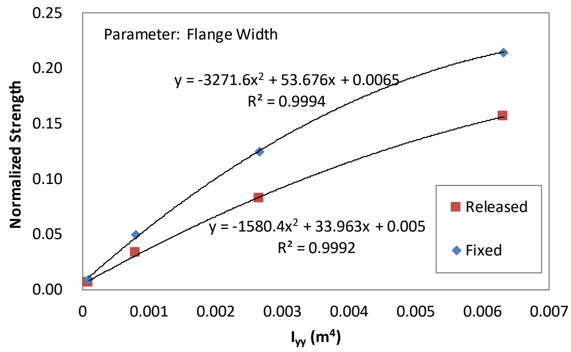

(b) Normalized strength vs I_{yy} varied by flange width

Fig. 10 Effect of I_{yy} on the buckling strength

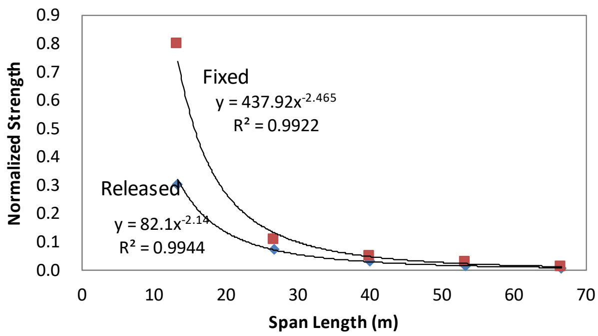

Fig. 11 Effect of span length on the normalized strength

girder buckling strength, the single girder equation can be used to estimate the buckling strength of a multi-girder system with released boundary conditions. However, if both ends are fixed in the abutment (most cases for IABs), then the single girder equation could not estimate the buckling strength conservatively.

4.2.3 Effect of moment of inertia (I_{yy})

The strong correlation between the moment of inertia (I_{yy}) and the buckling strength of the steel girder was found as shown in Fig. 9. The relationship between the maximum axial loads (buckling load) and I_{yy} shows a linear regression graph with a R-squared value of 0.99. If the points are divided in to two categories, one for the flange thickness and another for the flange width and redrawn for each case, logarithmic curves can be better fitted than linear curves. However, for larger moment of inertia, more analysis should be performed to find a better fitted curves.

Fig. 10 shows the results from each case by flange thickness or flange width. In this case, the R-squared value increases to greater than 0.99 for both the flange thickness and flange width. An increased normalized strength with an increased moment of inertia is better fitted with a natural logarithmic curve (ln) than a linear curve.

4.2.4 Effect of span length

The effect of span length on the normalized buckling strength of a steel girder without a deck is also compared as shown in Fig. 11.

The R-squared values for both fixed and released conditions are greater than 0.99. The strength with a varied span length can be described well by an exponential with an exponent to the power of -2.465 and -2.14 with coefficients of 436.92 and 82.1 respectively. These can be compared with the AISC buckling equation for a single girder if the span length is changed to a slenderness ratio.

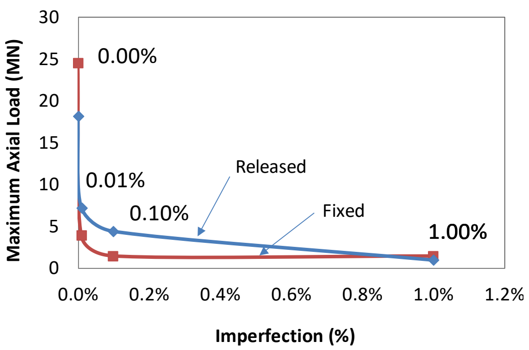

Fig. 12 Effect of the imperfection level on the buckling strength of a steel girder

4.2.5 Effect of imperfection

The effect of imperfection on the maximum axial load which is buckling strength is shown in Fig. 12.

For the released case, a 1.0% imperfection is the lowest value, while for the fixed case, 0.1% and 1.0% exhibited approximately the same strength. Other study shows the 0.1 or 0.033% of girder length for the imperfection of the steel girder bridge and sometimes the 10% to 0.2% of plate thickness for the imperfection of the steel structures (Thiébaud and Lebet 2014, Gardner and Chan 2007). However, based on simulation results, difference between 0.1 and 1.0% imperfection showed negligible changes. Therefore, from the behavior observed in both cases, it can be concluded that a 1.0% imperfection is an appropriate assumption to estimate the buckling strength of a steel girder conservatively.

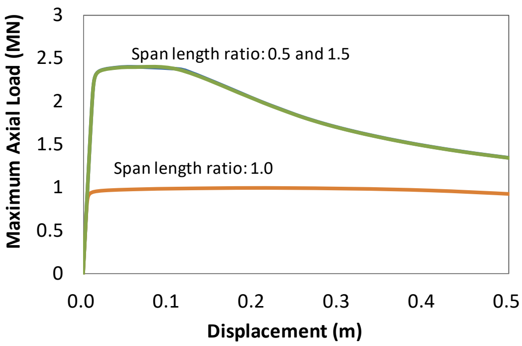

(a) Released condition

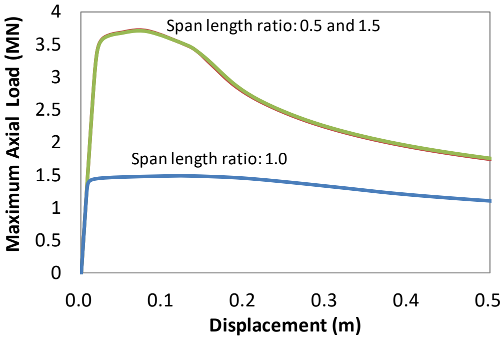

(b) Fixed condition

Fig. 13 Effect of the span ratio on the buckling strength of a steel girder

4.2.6 Effect of the span length ratio and self-weight

In this study, the effect of the span length ratio on the buckling strength was also studied. The span length ratio is defined as the ratio of the center span length to the outer span length. However, the total bridge length is the same as to 120 m no matter what the span ratio is in this study. In this study, a three-span continuous girder is investigated. It should be noted that most three span continuous IABs have center spans which are a little longer than the other two spans. Therefore, a 1.5 span ratio would be close to a more realistic condition in practice than a span-length ratio of 0.5. In this study, span-length ratios of both 0.5 and 1.5 were investigated. As previously mentioned, a span-length ratio of 0.5 means a 20 m-center span and a span of 50 m for the other two spans. Likewise, a span-length ratio of 1.5 means a 60 m center span and a 30 m length for the other two spans. Based on the results shown in Table 2, for both the released or fixed condition, as the span length ratio is decreased (0.5) or increased (1.5), increased maximum axial load (buckling strengths) were noted. The buckling mode shape changes with the span length ratio however as shown in Fig. 14. However, it should be noted that some studies (Olson *et al*. 2013, Holloway 2012) revealed that the longer center span (intermediate span) tends to increase the pile stress.

Buckling failure will occur at a critical span. If the effective length factor (K) and span length are known, the buckling failure point of each span can be found easily using a single column buckling equation as suggested by AISC. However, in a continuous beam with a multi-span, coupling effects between the adjacent spans affects the rotational stiffness of each span. Therefore, it is not trivial to estimate the effective length factor or the critical length. As shown in Fig. 14, the K value and the critical length can be estimated based on the results obtained from the post-buckling analysis. For the released condition, the outside span buckled, while for the fixed condition, the center span

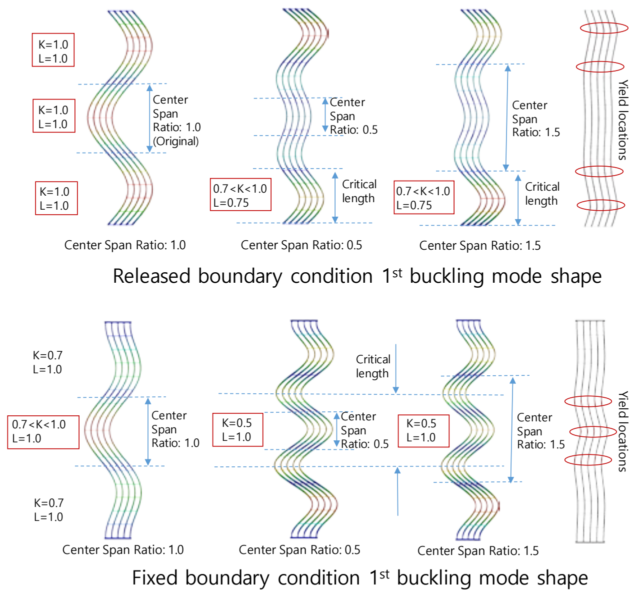

Fig. 14 Buckling mode shapes for different span length ratios

buckled no matter what the span length ratio was (0.5 or 1.5).

For the released boundary condition, the K value for the critical span (outer span) would be between 0.7 for a fixed condition and 1.0 for the released condition since one end of the span is connected to one end of another span, while the other end is free to rotate. For both the 0.5 and 1.5 span length ratio, the critical length was 0.75 (75%) compared to center span ratio 1.0 based on obtained results from post-buckling analysis. Therefore, the KL value for both the 0.5 and 1.5 cases should be between 0.525 and 0.75 respectively. The average of these two values is 0.64 and these are approximately considered as the KL values for both unequally spaced cases in a released condition. The obtained normalized strength for the released condition was 0.08. For an equally spaced bridge, with a span length of 27 m and a KL value of 0.66 exhibited a normalized strength of 0.074. It should be noted that the original span length of the bridge was 40 m. Therefore, based on this observation, the buckling strength for an unequally spaced girder can be easily estimated by using the KL value of the critical span.

For the fixed condition, in contrast to the released condition, the center span buckled as shown in Fig. 14. From the post-buckling analysis, it can be found that the critical length is close to 1.0, which is the original span length in the case of the fixed condition. The K value for the 0.5 and 1.5 span length ratios are considered to be 0.5 if buckling mode shapes are referred to. Therefore, KL can be estimated as being 0.5, which is lower than for the equally spaced case (0.7~1.0).

In this study, for released and fixed conditions, with a span length ratio of 0.5 and 1.5, KL values of 0.7 and 0.55 are recommended respectively, with a 10% safety margin. The self-weight of the steel girder was found to be a negligible factor in controlling the buckling failure.

4.3 Passive Earth pressure of soil

In this section, studies for estimating the passive earth pressure of soil from the abutment of IABs were reviewed. Lee *et al*. (2016) compared simulation results from a developed model with data from field research conducted by Lemnitzer *et al*. (2012) and found that the passive earth pressure generated can cause buckling in the weak axis of the steel girder during the summer season.

Field research data obtained from Lemnitzer *et al*. (2012) showed a passive earth pressure coefficient (K_P) from 10 to 24 when the backfill material consisted of well graded sand and gravel with 5 to 10% of SE 30 fill sand, which can be classified as SP and Group A-3 in the AASHTO soil classification.

For the passive earth pressure, there are wide range of studies which have a different view from Lemnitzer *et al*. (2012). Therefore, other research results regarding the passive earth pressure (K_P) generated by the expansion of the superstructure (movement of the backwall) due to temperature change were investigated. Clough and Duncun (NCHRP report 343) suggest the passive earth pressure (K_P) of 3.0 to 5.8 from loose sand to dense sand placed in backfill.

In experiments conducted by England *et al*. (2000) and Springman *et al*. (1996), most K_P values fall between 3.3 and 6.5, regardless of consideration of the wall friction. From field research, a fully passive pressure (K_P) of 6.2 was recorded from an integral backwall bridge (Hoppe and Gomez 1996). It should be noted that the passive earth pressure based on Rankine theory with conventional parameters (Coefficient of passive earth pressure (K_P): 3.6, φ (deg.): 34°, soil density (γ) 20.5 kN/m^3) could be much smaller than the field data obtained by Lemnitzer *et al*. (2012).

In the U.S., an integral bridge in West Lafayette, investigated by Frosch *et al*. (2009), confirmed that the earth pressure behind an abutment appeared to increase due to the densification of the soil by the ratcheting movement of backfill corresponding to bridge thermal movement. This indicates that the possibility of a buckling failure during deck replacement increases up to a certain age of the bridge. Although 318 m-long steel girder IAB has been built in U.S., the FHWA simply recommends using a limited span length of 91.4 m for the steel girder integral bridge. The UK recommends a maximum length of 60 m as a rule of thumb. New Zealand which is located in strong seismic zone only recommends that the distance between rear faces of abutment should be less than or equal to 70 m for concrete superstructures and 55m for steel superstructures (Wood *et al*. 2015). NY DOT recommends of using 140m limited span length for steel girder IABs which is the longest in US (Kunin and Alampalli 2000). However, these values are considered to be conservative and reasonable extension of these limitations could be achieved with detailed information and research work with consideration of buckling failure due to deck replacement in design.

BA 42/96 (Design manual for roads and bridges 2003) recommends using the equations shown below for the estimation of earth pressure when the abutment is of the shallow height bank pad and end screen type.

$$K^* = K_0 + (\frac{d}{0.025H})^{0.4}K_p \tag{1}$$

where, K_P is the passive earth pressure coefficient and K_0 is at the rest condition. 'd' is a thermal displacement on top of the abutment (multiplication factor 2) and H is a retained height. The live load surcharge and active earth pressure can be considered to be small and are ignored in BA 42/96 (2003). The results obtained with a fully passive pressure of between 3.3 and 6.2 are shown with consideration of K* value. According to Barker and Puckett (2013), the passive earth pressure can be obtained using the equation shown below.

$$K_p = 0.5 + 125\left(\frac{\Delta_{max}}{H}\right) \leq 3.0 \text{ (For Loose sand)} \tag{2}$$

The total earth pressure force on the abutment in the longitudinal axis of the bridge using K_P can easily be calculated. PennDOT DM4 (2015) uses the equation shown below.

$$F = 0.5\gamma K_p H^2 L \tag{3}$$

where, K_P is the passive earth pressure coefficient and γ is the unit weight of soil. H is the retained height and B is the

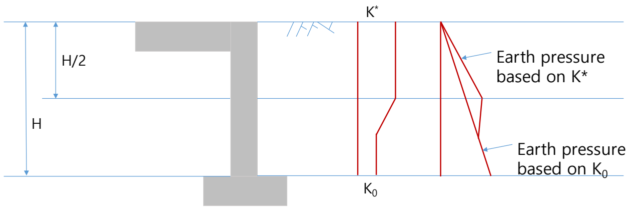

(a) Full height frame (BA 42/96)

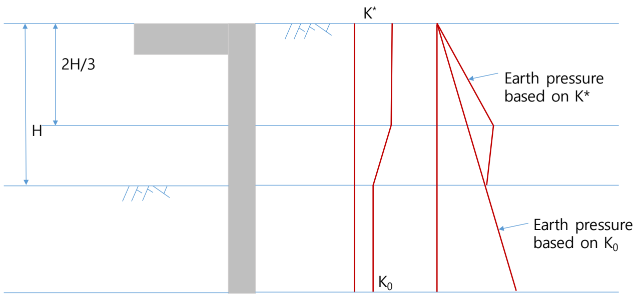

(b) Full height embedded wall abutment (BA 42/96)

Fig. 15 Earth pressure distribution along the depth of the abutment

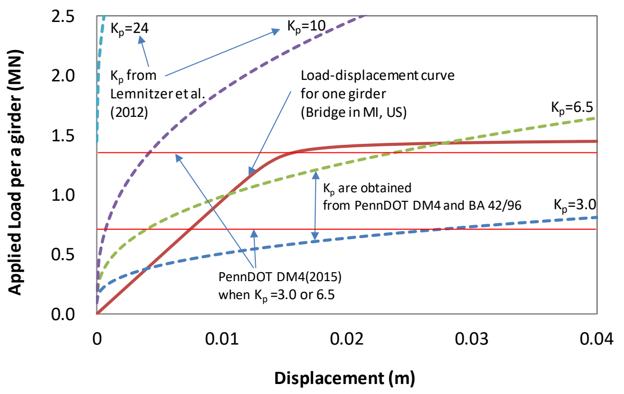

Fig. 16 Total earth pressure force and buckling strength

width of the abutment. It is assumed that there is no skew.

According to BA 42/96 (2003), K^* is considered as shown in Fig. 15.

For loose sand, the maximum passive earth pressure is limited to 3.0 as shown in Eq. (2). From Barker and Pucket (2013) for dense and medium dense sand, the maximum passive earth pressure is 5.8 and 4.0 respectively. These values are also selected in design manuals such as PennDOT DM4 and a study by Clough and Duncan (1991). These are also within a similar range with those K_P values (3.3-6.5) previously referred to from England *et al.* (2000) and Springman *et al.* (1996). Accordingly, in this study, to sum up, passive earth pressures from 3.0 up to 6.5 were considered and the results from Lemnitzer *et al.* (2012) were also compared.

Based on the proposed earth pressure distribution in BA 42/96 and Eqs. (1) and (3), with the assumed passive earth pressure (K_P = 3.0 – 6.5) and Lemnitzer's field research, the total earth pressure force (dotted line) and buckling strength (solid line) depending on the displacement of the top of the abutment can be drawn in one graph as shown in Fig. 16.

From the comparison seen in Fig. 16, when the BA42/96 equation is used with K_P values from PennDOT, it can be seen that for dense and medium dense sand, there was a possibility of buckling failure. However for loose sand (K_P = 3), buckling failure does not occur over the entire displacement. Similar results were obtained if the PennDOT equation (Eq. (3)) was used instead.

However, if the field data from Lemnitzer *et al.* (2012), is used (K_P = 10 or 24), then the selected steel girder becomes vulnerable to a buckling failure due to the high earth pressures. This indicates that between design guidelines such as BA42/96 and PennDOT DM4 and actual field measurement, there is significant gap. Further research work is therefore required. For estimation of end movement of the girder due to the temperature changes, Oesterle and Tabatabai (2014) recommended statistical factor for end movement of IABs. In order to design under the uncertainty of 98% confidence, end movement should be multiplied by factor of 1.6. In this study, the factor of movement was not considered.

4.4 Estimated maximum axial force for one girder (F_g)

The axial force in one steel girder of an IAB (F_g) due to thermal load can be practically estimated using the LTI equations (Eq. (4)) proposed by Laman and Kim (2009). Firstly the bridge compression force can be approximated using selected key parameters such as the thermal expansion coefficient (α), total bridge length (L), backfill height (H), backfill stiffness (B) and the pile-soil interaction (P). Laman and Kim (2009) recommend using a simple integer number for these parameters. For example, the backfill stiffness can be categorized into three grades; high (3.0), intermediate (2.0) and low (1.0). The equations were obtained based on long term field monitoring of IABs using several wireless measuring devices. A detailed explanation of this research works can be found in Laman and Kim (2009). The axial force acting on one steel girder (F_g) can be obtained simply as a value of the total bridge compression force (F_c) divided by the number of girders (Eq. (5)).

$$F_c = 4.45[-17.78\alpha - 6.56L - 59H \\ -101B + 16P + 374] \tag{4}$$

$$F_g = F_c / N_g \tag{5}$$

where:

F_c: bridge compression force (kN)
F_g single girder axial force (kN)
N_g: number of girders
α: thermal expansion coefficient (m/m/C°) × 1E-6
L: total bridge length (m)
H: backfill height (m)
B: backfill stiffness (normalized value (1 or 2 or 3))
P: pile-soil interaction (normalized value (1 or 2 or 3))
A_{one}: total area of one steel girder

The results obtained using the proposed equations are shown in Fig. 17. Both the single girder axial force due to

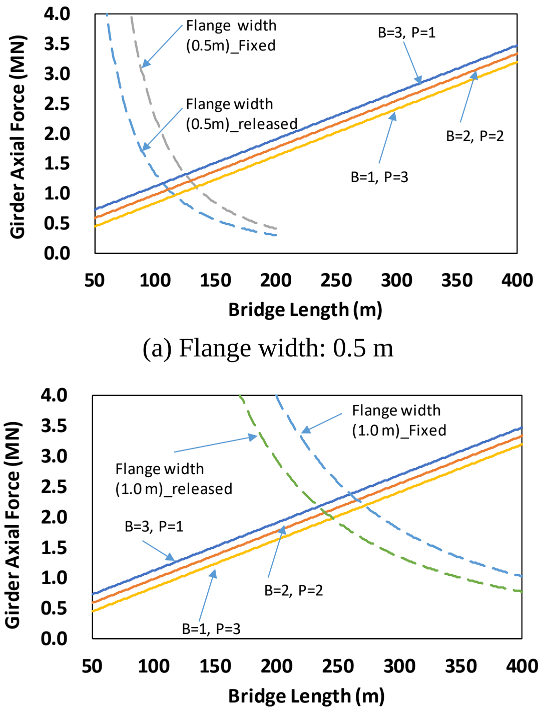

(a) Flange width: 0.5 m

(b) Flange width: 1.0 m

Fig. 17 Girder axial force and capacities against the bridge length

thermal loading (F_g) and the single girder capacity depending on the bridge length are shown in one graph. The axial force is indicated by the solid line and the girder capacity is indicated by the dotted line.

The proposed equations (Eqs. (1)-(5)) were used to check the possible buckling failure that could occur during deck removal. In this study, the imperfection level was assumed to be 1%. Both the section shown in Fig. 2 and a section with a 1.0 meter flange width were considered in order to see the differences in the girder capacity under axial load. The girder axial force estimated by the LTI equation under an intermediate condition (B = 2.0, P = 2.0) and both extreme cases (B = 1.0, P = 3.0 and B = 3.0, P = 1.0) were considered and are shown in one graph.

It can be found from Fig. 17 that the critical point for a 0.5 m flange width is located at a length of 120 m and axial force of 1,138 kN when a temperature variation of 17.8 degree Celsius (32 degree Fahrenheit) is present. For a 1.0 m flange width, the critical point is located at a length of 250 m and axial force of 2150 kN. In this study, the critical points were assumed to occur when both the B and P parameters are at an intermediate level and in a semi-fixed condition, which is an averaged value between fixed and released. Therefore, practically, if a 0.5 m flange width is used, the maximum bridge length can be considered as being 120 m. Similarly, if a 1.0 m flange width is used, the maximum bridge length can be considered as being 250 m. Cases for flange widths of between 0.5 m and 1.0 m can be estimated by using interpolation. Practically, it can be concluded that the flange width should be checked for deck replacement depending on the planned total length of the integral abutment bridge. However, under the local buckling criteria, 1.0 meter flange could be categorized non-compact section. For compact section with constant thickness (38.1 mm) as shown in Fig. 2, 0.655 m of flange width is the limit. Therefore, for plastic hinge behavior of the section (compact section), thickness of 1.0 meter flange should be increased.

The equation proposed based upon the LTI equation is solely based on an integral abutment bridge. However, during deck replacement in the summer season, the maximum temperature of the exposed steel girder could be much higher than the conditions considered in the equations in this study. Therefore, the equations for the temperature term should be modified for consideration of exposed girders in the sun. However, the effect of temperature changes on the LTI maximum axial force can be considered to be negligible. For example, the maximum temperature change that can occur in MI, USA is 117.4°F (65.2°C). For practical consideration, if half of that temperature change (59°F) is considered, for a 1.0 m and 0.5 m flange width, the critical point is located at a length of 245 m and 112 m respectively, which is similar value to the original equations (250 m and 120 m).

4.5 Proposed equation for the girder capacity

Lee *et al.* (2016) proposed an equation using regression analysis with the AISC buckling curve to estimate the buckling strength of IABs during deck replacement. Based on the findings of Lee *et al.* (2016), σ_{cr} can be obtained from coefficients regarding σ_{cr} such as *C*, *ex* and *I*. Based on equations from Lee *et al.* (2016), the further additional effect of the span length ratio is considered and the following equations for critical stress calculations (Eq. (6)) under passive earth pressure (Eqs. (7)-(9)) are developed.

$$\sigma_{cr} = C \times \sigma_y \times {\lambda_c}^{ex} \times I \times R \tag{6}$$

$$\sigma_{cr} A_{one} \, (or \; F_g) \geq 0.5\gamma K^* H^2 \times W_{bw} \; / \; N \tag{7}$$

$$\begin{aligned} &\sigma_{cr} A_{one} \left(or \; F_g\right) \geq \\ &\left[\left(\frac{\gamma H^2 K^*}{8}\right) + \left(\gamma H^2 K^* \left(\frac{K^*}{K_0} - 1\right)/2\right) \right. \\ &\left. + \left(\gamma H^2 \left(\frac{K^*}{2} + K_0\right)\left(1 - \frac{K^*}{2K_0}\right)/2\right)\right] W_{bw} \; / \; N \end{aligned} \tag{8}$$

$$\begin{aligned} &\sigma_{cr} A_{one} \left(or \; F_g\right) \geq \\ &\left\{(5\gamma H^2 K^*/9) + \left(\frac{\gamma H K^*}{3} + \frac{\gamma (H + H_e) K^*}{2}\right) H_e)\right\} W_{bw} \; / \; N \end{aligned} \tag{9}$$

$\sigma_{cr}A_{one} > F_g$, then use $\sigma_{cr}A_{one}$

$\sigma_{cr}A_{one} \leq F_g$, then use F_g

for comparison of the total earth pressure force.

where:

F_{cr}: Critical strength of the steel girder (MPa)

C: Boundary Coefficient

F_y: Yield strength of the steel girder (MPa)

λ_{cs} : Slenderness factor

ex : Exponent

I : Imperfection coefficient

For released at both ends:

I = -0.0030××imperfection level (%) + 0.929

For fixed at both ends:

I = -0.0034×Imperfection level (%) + 1.034

R: Span length ratio effects (valid when span length ratio is between 0.5 and 1.5)

For released conditions at both ends:

Use the effective length factor (K) = 0.7 for 0.5 and 1.5 span length ratio

For fixed conditions at both ends:

Use the effective length factor (K) = 0.55 for 0.5 and 1.5 span length ratio

For values between 0.5 and 1.5 span length ratio, use interpolation.

A_{one}: Cross sectional area of one steel girder (m^2)

K_0: At rest condition

K_p: Passive earth pressure coefficient

$$K^* = K_0 + \left(\frac{d}{0.025H}\right)^{0.4} K_p$$

for shallow height of abutment (less than 3 m)

$$K^* = K_0 + \left(\frac{d}{0.05H}\right)^{0.4} K_p$$

for full height portal frame abutment (less than 3 m)

$$K^* = K_0 + \left(\frac{d}{0.03H}\right)^{0.6} K_p$$

for full height portal frame abutment with hinge at the base (less than 3 m)

γ: Soil unit weight (kN/m^3)

H: Abutment height (m)

H_e: Embedded depth (m)

W_{bw}: Width of backwall (meters)

N : Number of girders in one IAB

F_g: Estimated maximum axial force proposed by LTI (kN)

The passive earth pressure and the corresponding reaction force from the backfill can be estimated from Eq. (7) to Eq. (9). Eq. (7) comes from PennDOT DM4 and Eq. (8) and Eq. (9) from BA42/96, in the distribution of the passive earth pressure coefficients. This load is also compared with the maximum axial force proposed by LTI and larger backfill force (total earth pressure force) can be used for the safety purposes. And finally, under plate local buckling criteria such as AISC specification (Table B4.1), width-thickness ratio should be checked.

5. Conclusions

1. Boundary effects from an adjacent span and the number of cycles in a critical span can be varied in continuous girder with multi-spans.
2. Most cross-frame exhibited a very low stress level (less than 6.22 MPa and 2.3 MPa for single and multi-girder respectively), indicating that cross-frame effects could be negligible and there was no torsional buckling due to the coupling effects between the multi-girders.
3. For a quick and conservative estimation of the girder buckling strength, a single girder equation can be used to estimate the buckling strength of a multi-girder system with released boundary conditions. However, if both ends are fixed in the abutment (most IAB cases), then the single girder equation could not estimate the buckling strength conservatively.
4. In this study, for released and fixed end conditions of IABs with span length ratios of 0.5 and 1.5, KL (effective length) values of 0.7 and 0.55 are recommended with a 10% safety margin in weak axis. Among design guidelines such as BA42/96, PennDOT DM4 and field measurement for passive earth pressures for IABs, there are significant gaps. Further research is required.
5. The LTI equation is solely based on an integral abutment bridge. However, during deck replacement in the summer season, the maximum temperature of the exposed steel girder could reach much higher than the conditions considered in the equations in this study. Further research on this issue such as thermal-mechanical coupled analysis should be conducted and incorporated with obtained results with this study.
6. It was found that if the width of the girder is 0.5 m, the maximum length of the bridge should be less than 120 m. This value could be used for practical applications as well as for design procedure of three span steel girder continuous IABs.
7. Proposed equation can be used for a bridge designer in order to determine an appropriate girder section size during deck replacement.

Acknowledgments

The authors gratefully acknowledge the support of Basic Science Research Program through the National Research Foundation of Korea (NRF) funded by the Ministry of Science, ICT and Future Planning (NRF-2015R1C1A1A02036617).

References

AASHTO Bridge design specifications (2015), AASHTO LRFD Bridge design specifications, American Association of State Highway and Transportation Officials, Washington, D.C., USA

ABAQUS (2015), ABAQUS/Explicit: User's Manual, Hibbitt Karlsson and Sorenson Inc., Pawtucket, RI, USA.

Ahn, J., Yoon, J., Kim, J. and Kim, S. (2011), "Evaluation on the behavior of abutment-pile connection integral abutment bridge", *J. Constr. Steel Res.*, **67**(7), 1134-1148.

AISC Manual of Steel Construction (2011), Manual of Steel Construction 14th Edition, American Institute of Steel Construction , Chicago, IL, USA.

BA42/96 (2003), The Design of Integral Bridges (Amendment No. 1), The Stationery Office, London, UK.

Baptiste, K., Kim, W. and Laman, J.A. (2011), "Parametric study and length limitations for prestressed concrete girder integral abutment bridges", *J. Int. Assoc. Bridge Struct. Eng.* (*IABSE*): *Struct. Eng. Int.*, **21**(2), 151-156.

Barker, R.M. and Puckett, J.A. (2013), *Design of Highway Bridges*: *An LRFD Approach*, (3rd Edition), John Wiley and Sons, Inc., New York, NY, USA.

Civjan, S.A., Kalayci, E., Quinn, B.H., Brena, S.F. and Allen, C.A. (2013), "Observed integral abutment bridge substructure response", *Eng*. *Struct*., **56**, 1177-1191.

Clough, G.W. and Duncan, J.M. (1991), *Earth Pressures*, Foundation Engineering Handbook, (2nd Edition), Edited by H.Y. Fung, Van Nostrand Reinhold, New York, NY, USA, pp. 223-235.

Dicleli, M. and Albhasi, S.M. (2004a), "Estimation of Length Limits for Integral Bridges Built on Clay", *J*. *Brdg*. *Eng*., **9**(6), 572-581.

Dicleli, M. and Albhasi, S.M. (2004b), "Effect of cyclic thermal loading on the performance of steel H-piles in integral bridges with stub-abutments", *J*. *Constr*. *Steel Res*., **60**(2), 161-182

England, G.L., Tsang, N.C.M. and Bush D.I. (2000), "Integral Bridges – A fundamental approach to the time temperature loading problem", Thomas Telford.

Faraji, S., Ting, J.M., Crovo, D.S. and Ernst, H. (2001), "Nonlinear analysis of integral bridges: finite-element model", *J*. *Geotech*. *Geoenvirn*., **127**(5), 454-461.

Frosch, R.J., Kreger, M.E. and Talbott, A.M. (2009), "Earthquake resistance of integral abutment bridges", FHWA / IN / JTRP-2008/11; Joint Transportation Research Program, Indiana Department of Transportation and Purdue University, IN, USA.

Gardner, L., and Chan, T.M. (2007), "Cross-section classification of elliptical hollow sections", *Steel Compos*. *Struct*., *Int*. *J*., **7**(3), 185-200.

Holloway, K.P. (2012), "Illinois integral abutment bridges: behavior under extreme thermal loading and design recommendations", M.S. Thesis; University of Illinois at Urbana-Champaign, IL, USA.

Husain, I. and Bagnariol, D. (2000), "Design and performance of jointless bridges in ontario: new technical and material concepts", *Transport*. *Res*. *Rec*., **1696**, 109-121.

Kim, W. and Laman, J.A. (2011), "Seven-Year Field Monitoring of Four Integral Abutment Bridges", *J*. *Perform*. *Constr*. *Facility*, **26**(1), 54-64.

Kim, W., Laman, J.A. and Linzell, D.G. (2012), "Prediction of concrete integral abutment bridge unrecoverable displacements", *ACI Special Publication* (*SP*)*-284*, **284**(11), 1-20.

Kim, W. and Laman, J.A. (2013), "Integral abutment bridge behavior under uncertain thermal and time-dependent load", *Struct*. *Eng*. *Mech*., *Int*. *J*., **46**(1), 53-73.

Kunin, J. and Alampalli, S. (2000), "Integral abutment bridges: Current practice in United States and Canada", *J*. *Perform*. *Constr*. *Facility*, **14**(3), 104-111

LaFave, J.M., Riddle, J.K., Jarrett, M.W., Wright, B.A., Svatora, J.S., An, H. and Fahnestock, L.A. (2016), "Numerical simulations of steel integral abutment bridges under thermal loading", *J*. *Bridge Eng*., **21**(10).

Laman, J.A. and Kim, W. (2009), "Monitoring of Integral Abutment Bridges and Design Criteria Development", Report No. FHWA-PA-2009-005-PSU002: The Thomas D. Larson Pennsylvania Transportation Institute, Pennsylvania Transportation Research Council, Harrisburg, PA, USA

Lemnitzer, A., Hilson, C., Taciroglu, E., Wallace, J.W. and Stewart, J.P. (2012), "Effect of backfill relative density on lateral response of a bridge abutment wall", *Proceedings of the 15th World Conference on Earthquake Engineering*, Lisbon, Porutugal, September.

Lee, J., Jeong, Y. and Kim, W. (2016), "Steel girder buckling in integral abutment bridges during deck replacement", *Int*. *J*. *Steel Struct*., **16**(4), 1071-1082.

Lock, R.J. (2002), "Integral Bridge Abutment" CUED/D-SOILS/TR320; M. Eng. Project Report, Cambridge, UK

Memon, B.A. and Su, X. (2004), "Arc-length technique for nonlinear finite element analysis", *J*. *Zhejiang Univ*. *Sci*., **5**(5), 618-628.

Oesterle, R.G. and Tabatabai, H. (2014), "Design considerations for integral abutment Jointless Bridges in the USA", Civil and Environmental Engineering Faculty Articles. http://dc.uwm.edu/cee_facart/1

Olson, S.M., Holloway, K.P., Buenker, J.M., Long, J.H. and LaFave, J.M. (2013), "Thermal behavior of IDOT integral abutment bridges and proposed design modifications", Illinois Center for Transportation, Research Report FHWA-ICT-12-022.

PennDOT Design Manual (2015), PennDOT Design Manual Part 4 (DM4), Commonwealth of Pennsylvania, Department of Transportation, Harrisburg, PA, USA

Pugasap, K., Kim, W. and Laman, J.A. (2009), "Long-term response prediction of integral abutment bridges", *J*. *Brdg*. *Eng*., **14**(2), 129-139.

Ramm, E. (1981), "Strategies for Tracing the Nonlinear Response near Limit Points", *Proceedings of Europe-U.S. Workshop on Non-linear Finite Element Analysis in Structural Mechanics*, Springer-Verlag, Germany, July.

Riks, E. (1972), "The application of Newton's method to the problem of elastic stability", *J*. *Appl*. *Mech*., **39**(4), 1060-1065.

Riks, E. (1979), "An incremental approach to the solution of snapping and buckling problems", *Int*. *J*. *Solids Struct*., **15**(7), 529-551.

Roeder, C.W. (2002), "Thermal movement design procedure for steel and concrete bridges", Report No. NCHRP 20-07/106: National Cooperative Highway Research Program, Washington, D.C., USA.

Springman, S.M., Norrish, A. and Ng, C.W.W. (1996), Cyclic loading of sand behind integral bridge abutments; TRL Project Report 146. Crowthorne: Transport Research Laboratory.

Thiébaud, R. and Lebet, J.P. (2014), "Resistance to LTB of steel bridge girders", *Proceedings of the 7th European Conference on Steel and Composite Structures*, No. EPFL-CONF-202635, pp. 759-760.

Wempner, G.A. (1971), "Discrete approximation related to nonlinear theories of solids", *Int*. *J*. *Solids Struct*., **7**(11), 1581-1599.

William, G.W., Shoukry, S.N. and Riad, M.Y. (2012), "Study of thermal stresses in skewed integral abutment steel girder bridges", *Struct*. *Eng*. *Int*., **22**(3), 308-317.

Wood, J., Murashev, A., Palermo, A., Al-Ani, M., Andisheh, K. and Goodall, D. (2015), "Criteria and guidance for the design of integral bridges in New Zealand", NZ Transport Agency Research Report 577.

CC